

generator output has a center frequency of 5.8 GHz with -49 dBm/MHz amplitude at 200-MHz PRF.

REFERENCES

1. H. Xie, X. Wang, A. Wang, B. Zhao, Y. Zhou, B. Qin, H. Chen, and Z. Wang, A varying pulse width 5th-derivative Gaussian pulse generator for UWB transceivers in CMOS, IEEE Radio and Wireless Symposium, 2008, 171–174.
2. H. Kim, Y. Joo, and S. Jung, A tunable CMOS UWB pulse generator, IEEE International Conference on Ultra-Wideband, 2006, 109–112.
3. S. Choobkar and A.J. Nabavi, A low power programmable CMOS circuit for generating modulated pulses for UWB applications, The 2nd International Conference on Wireless Broadband and Ultra Wideband Communications, 2007, 5–5.
4. Y. Zhu, J.D. Zuegel, J.R. Marciano, and H. Wu, Distributed waveform generator: A new circuit technique for ultra-wideband pulse generation, shaping and modulation, IEEE J Solid-State Circuits 44 (2009), 808–823.
5. S. Bourdel, Y. Bachelet, J. Gaubert, R. Vauche, O. Fourquin, N. Dehaese, and H. Barthelemy, A 9-pJ/Pulse 1.42-Vpp OOK CMOS UWB pulse generator for the 3.1–10.6-GHz FCC band, IEEE Trans Microwave Theory Tech 58 (2010), 65–73.
6. J. Lee, Y.-J. Park, M. Kim, C. Yoon, J. Kim, and K.-H. Kim, System-on-package ultra-wideband transmitter using CMOS impulse generator, IEEE Trans Microwave Theory Tech 54 (2006), 1667–1674.
7. M. Demirkan and R.R. Spencer, A pulse-based ultra-wideband transmitter in 90-nm CMOS for WPANs, IEEE J Solid-State Circuits 43 (2008), 2820–2828.
8. Y. Jeong, S. Jung, and J. Liu, A CMOS impulse generator for UWB wireless communication systems, International Symposium on Circuits and Systems, 2004, 129–132.
9. F. Demeestere, C. Delaveaud, and J. Keignart, A compact UWB antenna with a wide band circuit model and a time domain characterization, IEEE International Conference on Ultra-Wideband (2006), 345–350.

© 2011 Wiley Periodicals, Inc.

SURFACE-MOUNT WWAN MONOPOLE SLOT ANTENNA FOR MOBILE HANDSET

Kin-Lu Wong and Po-Wei Lin

Department of Electrical Engineering, National Sun Yat-Sen University, Kaohsiung 804, Taiwan; Corresponding author: wongkl@ema.ee.nsysu.edu.tw

Received 6 November 2010

ABSTRACT: A surface-mount monopole slot antenna with a small volume of $13 \times 28.5 \times 2.2 \text{ mm}^3$ for penta-band wireless wide area network operation in the mobile handset is presented. The antenna is to be surface-mounted at a rectangular notch of size $13 \times 28.5 \text{ mm}^2$ near the bottom edge of the system ground plane. When surface-mounted, the antenna is closely integrated with surrounding system ground plane on the main circuit board of the handset. The antenna can provide two wide operating bands of 824–960 and 1710–2170 MHz to respectively cover the GSM850/900 and GSM1800/1900/UMTS operations. The surface-mount antenna mainly comprises a monopole slot of width 4 mm and length 50 mm, which is bent to have a compact size and is fed by a microstrip feedline. Both the monopole slot and microstrip feedline are printed on two opposite surfaces of a dielectric substrate, which is bent into an inverted-U shape for surface-mounting on the circuit board of the handset. Details of the proposed antenna are described, and results of the antenna including its specific absorption rate values are presented and discussed. © 2011 Wiley Periodicals, Inc. Microwave Opt Technol Lett 53:1890–1896, 2011; View this article online at wileyonlinelibrary.com. DOI 10.1002/mop.26096

Key words: internal handset antennas; mobile antennas; monopole slot antennas; WWAN antennas; surface-mount antennas

1. INTRODUCTION

On-board printed monopole slot antennas or known as quarter-wavelength slot antennas for penta-band wireless wide area network (WWAN) operation in the 824–960 MHz band (GSM850/900) and 1710–2170 MHz band (GSM1800/1900/UMTS) for mobile handset applications has been reported [1–3]. Such monopole slot antennas are to be directly printed on the main circuit board of the mobile handset and are mainly operated at their quarter-wavelength resonant modes [1–10], different from the traditional slot antennas operated at the half-wavelength resonant mode [11–14], thus resulting in decreased antenna size. This attractive feature makes it very promising for applications in the mobile communication devices such as the laptop computers, tablet computers, mobile handsets, and so forth. For bar-type handset applications, two monopole slots of different lengths are required to provide two wide operating bands to cover penta-band WWAN operation [1].

For clamshell or folder-type handset applications [2], a single monopole slot antenna printed on the top portion of the main circuit board and placed at the hinge of the handset can generate two wide operating bands for penta-band WWAN operation. In this case, wideband operation is obtained mainly because dipole-like chassis resonant modes contributed by the two ground planes of the clamshell handset are generated, which greatly enhances the operating bandwidths of the antenna. Likewise, by embedding the monopole slot antenna at the center of the system ground plane printed on the main circuit board of the bar-type handset [3], the dipole-like chassis resonant mode of the system ground plane can also be excited to assist in forming a wide operating band to cover penta-band WWAN operation. However, this layout will complicate the circuit floor planning and signal line routing on the main circuit board [3], which is less attractive for practical handset applications.

It is also noted that for the reported monopole slot antennas, they are generally to be directly printed on the main circuit board of the handset [1, 3, 15–17]. This makes the antenna easy to fabricate at low cost. However, on the other hand, it is inconvenient for the dimensions of the printed slot antenna to be post-adjusted to fine-tune the operating bandwidths of the antenna. The postadjustment may be required in some cases to compensate for the possible coupling between the embedded antenna and the nearby electronic elements mounted inside the handset, which may cause some frequency shifting in the antenna's operating bandwidths.

To overcome the problem, we propose in this study a promising surface-mount monopole slot antenna for WWAN operation in the mobile handset. The proposed antenna comprises a single monopole slot and a microstrip feedline, both printed on two opposite surfaces of a dielectric substrate. The antenna occupies a small volume of $13 \times 28.5 \times 3 \text{ mm}^3$ (about 1.1 cm^3) for pentaband WWAN operation. The antenna is to be surface-mounted at a rectangular notch of size $13 \times 28.5 \text{ mm}^2$ (about 370 mm^2) near the bottom edge of the system ground plane. The distance between the antenna and the bottom edge of the system ground plane is 15 mm only. In addition, the ground portion between the antenna and the bottom edge of the system ground plane can be used to accommodate associated electronic elements in the handset. This leads to compact integration of the proposed antenna in the handset and also minimizes the antenna effects on the circuit floor planning and signal line routing on

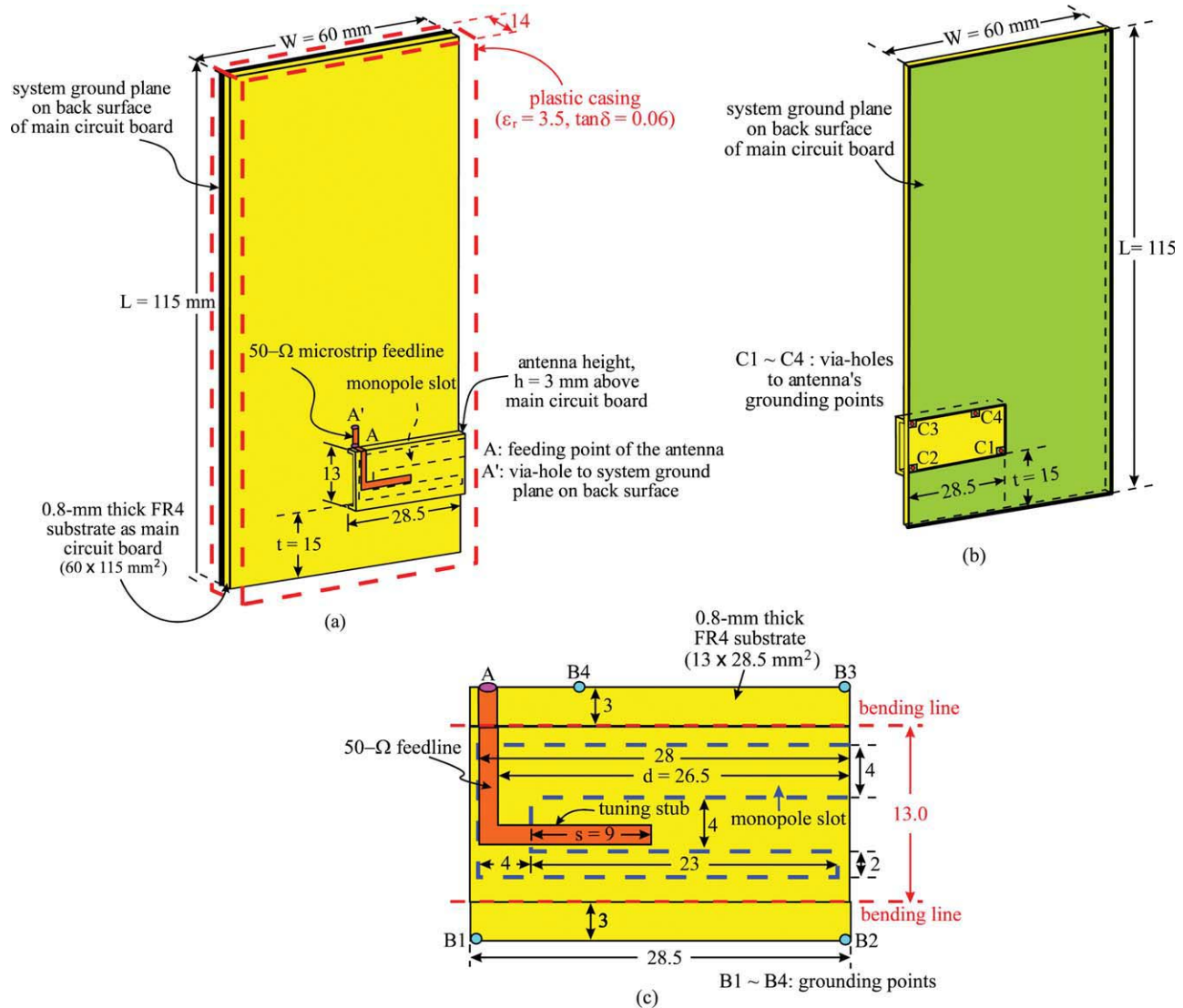


Figure 1 (a) Geometry of the surface-mount WWAN monopole slot antenna mounted on the front surface of the main circuit board of the mobile handset. (b) Geometry of the main circuit board (back view). (c) Dimensions of the surface-mount monopole slot antenna in its unbent structure. [Color figure can be viewed in the online issue, which is available at wileyonlinelibrary.com]

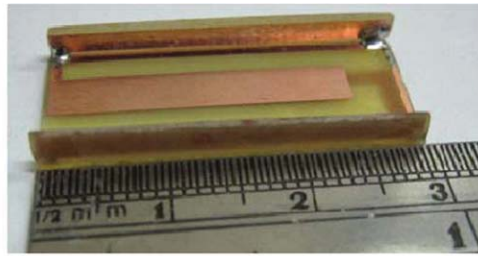
the main circuit board. Also note that by mounting the antenna near the bottom edge of the main circuit board, the specific absorption rate (SAR) [18] values can be greatly decreased, making it easy to meet the limit of 1.6 W/kg for 1-g head tissue [19–24]. Details of the proposed antenna are presented.

2. PROPOSED SURFACE-MOUNT MONOPOLE SLOT ANTENNA

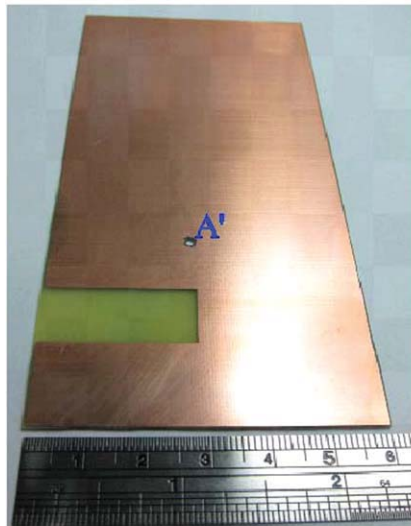
Figure 1(a) shows the geometry of the proposed surface-mount WWAN monopole slot antenna for mobile handset. The antenna is mounted above a rectangular notch of size $13 \times 28.5 \text{ mm}^2$ near the bottom edge of the system ground plane [see Fig. 1(b)], which is printed on the back surface of the main circuit board. The distance (t) between the rectangular notch and the bottom edge of the main circuit board is 15 mm, and the ground portion in this region can be used to accommodate associated electronic elements such as a universal series bus connector [25] to serve as a data port for external devices [26], the lens of an embedded digital camera [27, 28], and so forth. Also note that an FR4 substrate of relative permittivity 4.4, loss tangent 0.02, thickness

0.8 mm, length (L) 115 mm, and width (W) 60 mm is used as the main circuit board in the study. To simulate the mobile handset casing in practical applications, a plastic casing made by a plastic material of relative permittivity 3.5, loss tangent 0.06, and thickness 1 mm encloses the main circuit board and the surface-mount antenna thereon. The overall thickness of the plastic casing is 14 mm, and the main circuit board inside the casing is of about the same distance to both sides of the plastic casing.

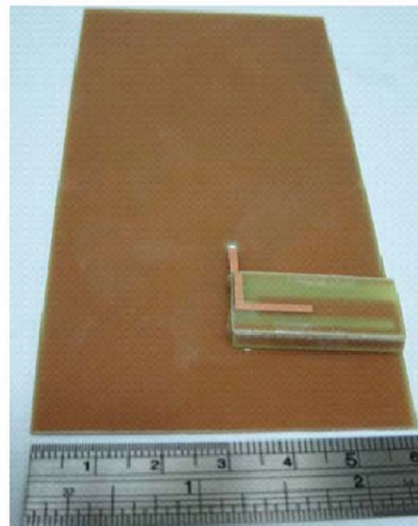
Detailed dimensions of the surface-mount monopole slot antenna in its unbent structure are given in Figure 1(c). The monopole slot is fed by a 50-Ω microstrip feedline. Both the monopole slot and microstrip feedline are printed on the opposite surfaces of the dielectric substrate, which is an FR4 substrate of relative permittivity 4.4, loss tangent 0.02, and thickness 0.8 mm in the study. The dielectric substrate is bent into an inverted-U shape for surface-mounting on the main circuit board. The front end of the microstrip feedline is Point A, which is the feeding point of the antenna. When the antenna is surface-mounted on the main circuit board, Point A is connected to a short 50-Ω microstrip feedline printed on the front surface of the



Surface-mount monopole slot antenna



Back view of main circuit board



Front view of main circuit board and the antenna

A': via-hole to connect the 50-ohm microstrip feedline to a 50-ohm SMA connector (not shown in the photo)

Figure 2 Photos of the fabricated antenna. Plastic casing not shown in the photos. [Color figure can be viewed in the online issue, which is available at wileyonlinelibrary.com]

main circuit board, which is then connected through a via-hole at Point A' to a 50- Ω SMA connector on the back surface of the main circuit board for testing the antenna in the experiment.

The monopole slot has a length of 59 mm and is bent into a C-shape to achieve a compact size of the antenna. The length 59 mm is close to about 0.18 wavelength of the frequency at 900 MHz. As it is printed on a dielectric substrate, which reduces the resonant length of the monopole slot, the antenna can generate a quarter-wavelength resonant mode at about 900 MHz and a half-wavelength resonant mode at about 1900 MHz. The two resonant modes form the antenna's lower and upper bands to respectively cover the GSM850/900 (824–894/880–960 MHz) and GSM1800/1900/UMTS (1710–1880/1850–1990/1920–2170 MHz) operations. In addition, note that the bent monopole slot is arranged to be on the central portion of the surface-mount antenna, and the two side portions of the antenna are with the ground plane only, whose grounding points (Points B1 to B4) are connected to the system ground plane on the main circuit board through via-holes at Points C1 to C4. In this case, nearby electronic components mounted on the main circuit board can be placed very close to or in direct contact with the surface-mount antenna such that compact integration of the surface-mount antenna inside the mobile handset can be obtained. This behavior is similar to the property of the EMC internal handset antennas [28–31], which has vertical ground planes connected to the system ground plane of the mobile handset.

Also note that the microstrip feedline passes the monopole slot at a distance (d) of 26.5 mm to the slot's open end, which is at about the center of the monopole slot. The distance d is an important factor in exciting the two desired resonant modes of the monopole slot. The length s of the tuning stub of the microstrip feedline is selected to be 9 mm, which also affects the

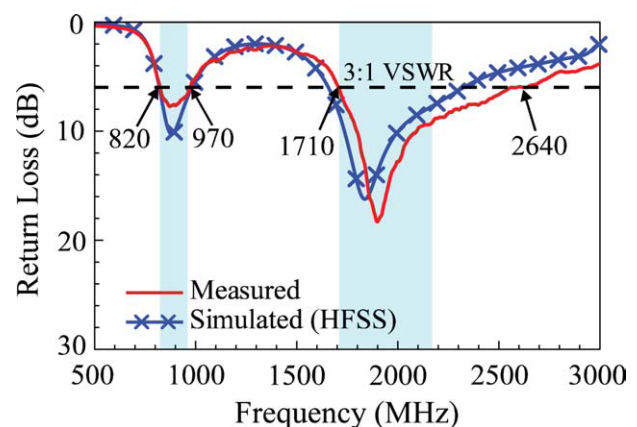


Figure 3 Measured and simulated return loss of the antenna. [Color figure can be viewed in the online issue, which is available at wileyonlinelibrary.com]

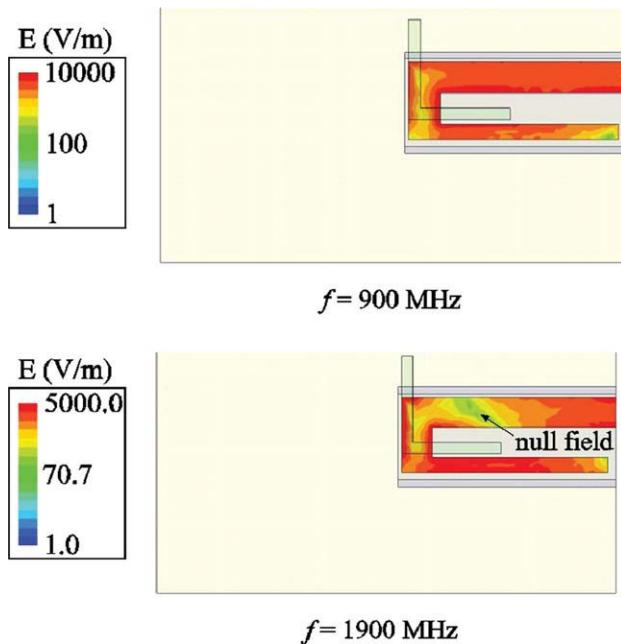


Figure 4 Simulated electric-field distributions at 900 and 1900 MHz in the monopole slot. [Color figure can be viewed in the online issue, which is available at wileyonlinelibrary.com]

impedance matching of the excited resonant modes. A parametric study of the major parameters will be presented in Section 3.

3. RESULTS AND DISCUSSION

The surface-mount monopole slot antenna was fabricated and tested. Figure 2 shows the photos of the fabricated antenna and the main circuit board in the experiment. Results of the measured and simulated return loss of the antenna are shown in Figure 3. The simulated results are obtained using simulation software high frequency structure simulator version 12 [32], and agreement between the measurement and simulation is observed. Results showed that two wide operating bands are obtained. The impedance matching for frequencies over the desired lower band (824–960 MHz) and upper band (1710–2170 MHz) is all better than 3:1 VSWR (6-dB return loss), which is widely used as the design specification for the internal WWAN handset antenna.

To analyze the excited resonant modes of the monopole slot, Figure 4 shows the simulated electric-field distributions at 900 and 1900 MHz in the monopole slot. At 900 MHz, the maximum field occurs at the open end and then decreases toward the closed end, which is similar to that of the excited quarter-wavelength slot resonant mode [10, 33]. Although at 1900 MHz, there is a null field at about the center of the monopole slot, indicating that a quarter-wavelength slot resonant mode is excited.

Figure 5 shows the measured three-dimensional total-power radiation patterns for the antenna. At each frequency, four radiating patterns seen in different directions (the top, bottom, front, and back directions) are shown. For lower frequencies at 859 and 925 MHz, half-wavelength dipole-like radiation patterns are observed. For higher frequencies at 1795, 1920, and 2045 MHz, the radiation patterns are close to full-wavelength dipole-like patterns with a dip in the azimuthal plane (x - y plane) of the radiation patterns. The obtained radiation patterns are similar to those of many reported internal WWAN handset antennas. This indicates that the system ground plane in this study is also a

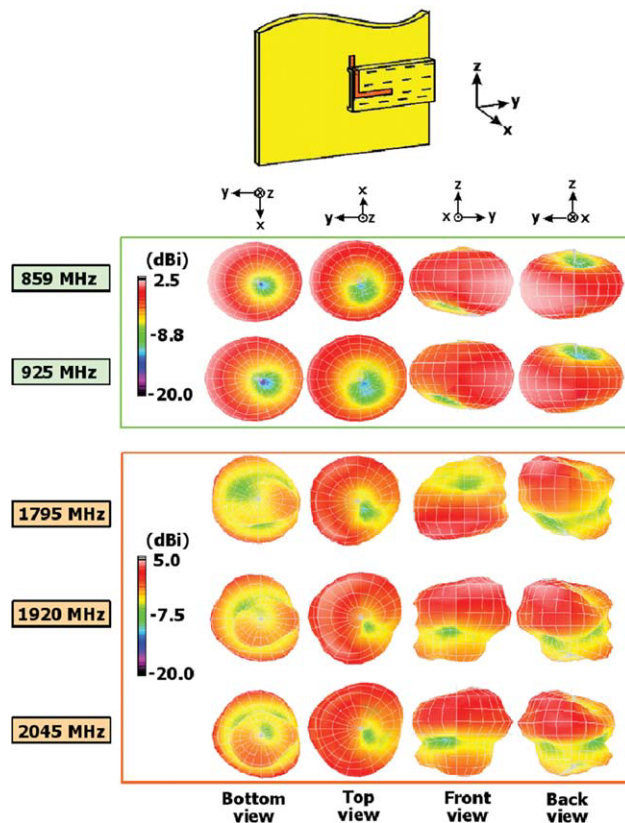


Figure 5 Measured three-dimensional total-power radiation patterns for the antenna. [Color figure can be viewed in the online issue, which is available at wileyonlinelibrary.com]

part of the radiator and contributes significantly to the radiation characteristics of the mobile handset [34]. The measured antenna efficiency (mismatching loss included) of the antenna is presented in Figure 6. The antenna efficiency varies from about 55 to 78% over the GSM850/900 bands and about 70 to 85% over the GSM1800/1900/UMTS bands. The obtained far-field radiation characteristics are acceptable for practical handset applications.

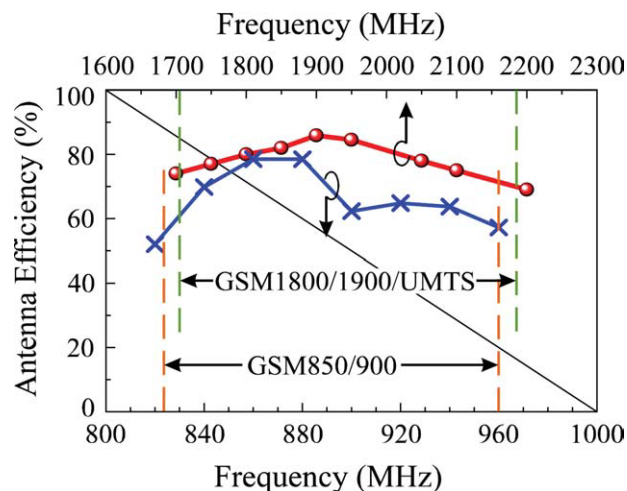
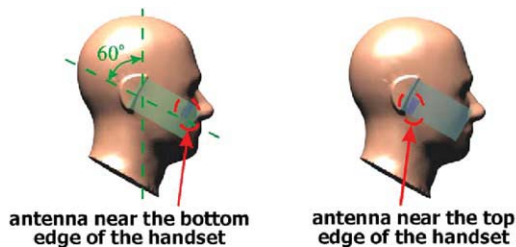


Figure 6 Measured antenna efficiency (mismatching loss included) for the antenna. [Color figure can be viewed in the online issue, which is available at wileyonlinelibrary.com]



Antenna location	f (MHz)	859	925	1795	1920	2045
Near bottom edge	1-g SAR (W/kg)	0.91	0.92	0.68	0.62	0.53
	Return loss (dB)	8.6	7.8	12.8	14.8	11.0
Near top edge	1-g SAR (W/kg)	1.35	1.27	1.27	1.05	0.85
	Return loss (dB)	12.0	10.4	11.4	9.1	7.4

Figure 7 SAR simulation model and the simulated 1-g SAR values. [Color figure can be viewed in the online issue, which is available at wileyonlinelibrary.com]

Figure 7 shows the SAR simulation model and the simulated 1-g SAR values. The return loss at each testing frequency is also given. The SAR simulation model is provided by SEMCAD X version 14 [35]. In addition to the antenna mounted near the bottom edge of the handset, the case for the antenna near the top edge of the handset is also studied. For the two cases, the obtained SAR values are all less than 1.6 W/kg [18], indicating that the antenna is promising for practical handset applications. Also note that when the antenna is mounted near the bottom edge of the handset, the obtained SAR values are lower, which is largely because the excited surface currents on the system ground plane are stronger near the antenna and agrees with the observations of other internal WWAN antennas mounted at the bottom edge of the handset [20, 21].

A parametric study is also conducted. Figure 8 shows the simulated return loss as a function of the distance t of the antenna to the bottom edge of the main circuit board. Results for the distance t varied from 10 to 20 mm are presented. When the distance t is smaller ($t = 10$ mm in the figure), the obtained bandwidths of the lower band are decreased. The decreased

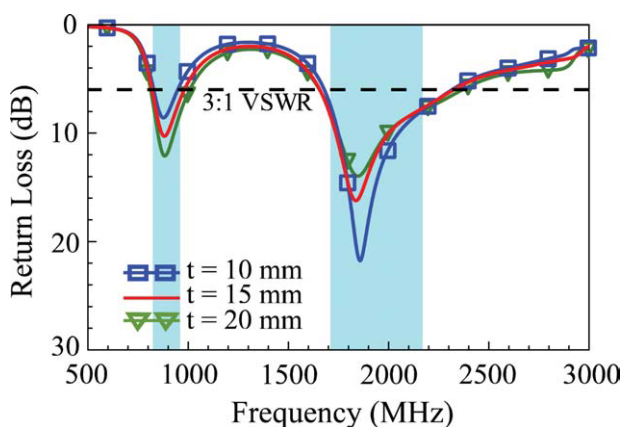


Figure 8 Simulated return loss as a function of the distance t of the antenna to the bottom edge of the main circuit board. [Color figure can be viewed in the online issue, which is available at wileyonlinelibrary.com]

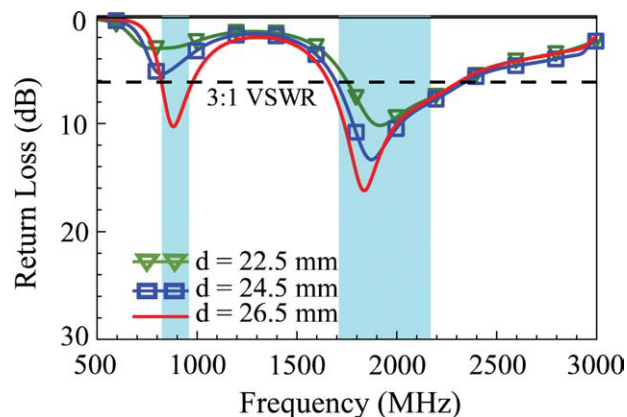


Figure 9 Simulated return loss as a function of the feeding position d of the microstrip feedline. Other dimensions are the same as in Figure 1. [Color figure can be viewed in the online issue, which is available at wileyonlinelibrary.com]

bandwidths are owing to the decreased upper-edge frequencies with 6-dB return loss for the lower band, with their corresponding lower-edge frequencies with 6-dB return loss about the same. This behavior is largely as the two ground portions separated by the rectangular notch is more asymmetric for smaller distances of t such that the dipole-like chassis resonant mode of the system ground plane cannot be excited effectively to assist in achieving widened bandwidths of the lower band. On the other hand, when the distance t is large ($t = 20$ mm in the figure), widened bandwidths are obtained for the lower band. For the upper band, however, the obtained bandwidths are about the same for the length t varies from 10 to 20 mm. That is, effects of the length t are not significant on the upper-band bandwidth.

Figure 9 shows the simulated return loss as a function of the feeding position d of the microstrip feedline. Other dimensions are the same as in Figure 1. Results for the feeding position d varied from 22.5 to 26.5 mm are shown in the figure. Strong effects on the two excited resonant modes of the monopole slot are seen. This indicates that the selection of the proper feeding position is important in the proposed antenna, and the preferred feeding position is at $d = 26.5$ mm, which is close to the center of the monopole slot.

Effects of the tuning-stub length s of the microstrip feedline are also studied. Figure 10 shows the simulated return loss for the tuning-stub length s varied from 9 to 11 mm. Large effects on the lower band of the antenna are observed. By selecting a proper length of the tuning stub, widened bandwidth for the lower band can be obtained. On the other hand, effects on the antenna's upper band are relatively very small.

Figure 11 shows the simulated return loss as a function of the antenna height h above the main circuit board. Other dimensions are the same as in Figure 1. Results of the simulated return loss for h varied from 0 to 4 mm are presented. For $h = 0$ (the monopole slot directly in contact with the main circuit board), small effect is seen for the lower band at about 900 MHz. However, large effect on the upper band is observed, and the upper-band bandwidth is quickly decreased and cannot cover the 1710–2170 MHz band. For $h = 2, 3,$ and 4 mm (that is, there is an air-layer spacing between the monopole slot and the main circuit board), the obtained upper-band bandwidths are increased with an increase in the antenna height h . The results indicate that the presence of the air-layer spacing between the printed monopole slot and the main circuit board can lead to

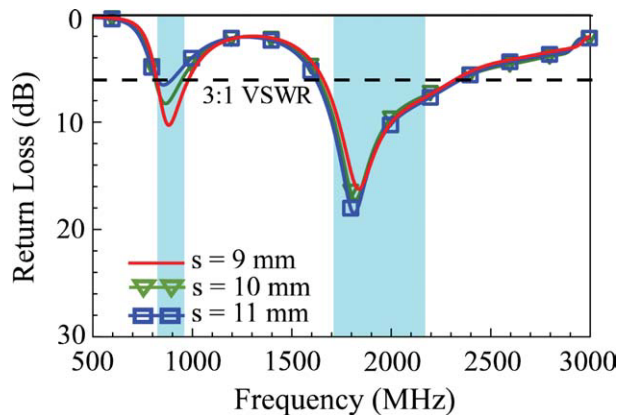


Figure 10 Simulated return loss as a function of the tuning-stub length s of the microstrip feedline. Other dimensions are the same as in Figure 1. [Color figure can be viewed in the online issue, which is available at wileyonlinelibrary.com]

larger upper-band bandwidth obtained for the antenna, with the lower-band bandwidths about the same. This behavior is largely because when the antenna is directly mounted on the main circuit board, there will be some additional dielectric loading on the printed monopole slot of the surface-mount antenna, which degrades the obtained bandwidth of the antenna, especially the upper-band bandwidth.

Figure 12 shows the simulated return loss as a function of the length L and width W of the main circuit board. Other dimensions are the same as in Figure 1. Results of the simulated return loss for the length L varied from 105 to 125 mm are shown in Figure 12(a), and those for the width W varied from 40 to 60 mm are presented in Figure 12(b). Results show that widened bandwidths for the lower and upper bands can be obtained when the width W is decreased. This behavior is largely because with a smaller width W of the main circuit board, the two ground portions of the system ground plane separated by the rectangular notch will become connected through a narrower metal portion such that the dipole-like chassis resonant mode contributed by the system ground plane becomes easier to be excited to help achieve a wider bandwidth. For the variations in the length L , however, the effects on the obtained bandwidths are not significant, and the bandwidths for all the lengths in the figure can cover the desired penta-band WWAN operation. This

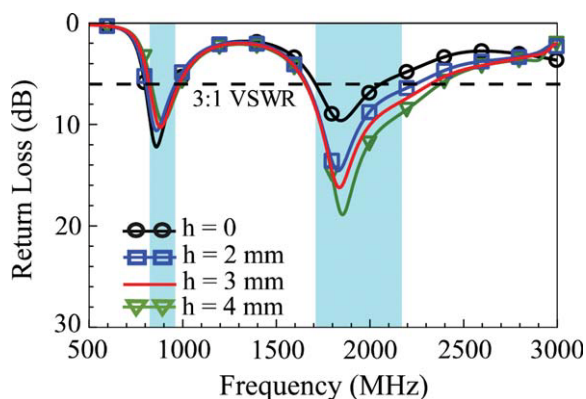


Figure 11 Simulated return loss as a function of the antenna height h above the main circuit board. Other dimensions are the same as in Figure 1. [Color figure can be viewed in the online issue, which is available at wileyonlinelibrary.com]

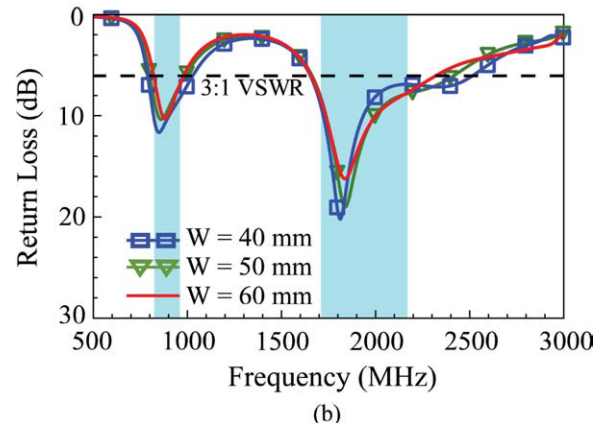
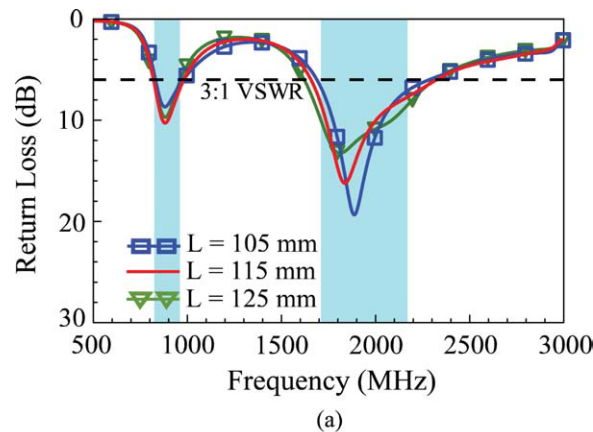


Figure 12 Simulated return loss as a function of (a) the length L and (b) the width W of the main circuit board. Other dimensions are the same as in Figure 1. [Color figure can be viewed in the online issue, which is available at wileyonlinelibrary.com]

is an attractive feature for the proposed monopole slot antenna in practical applications.

4. CONCLUSIONS

A new surface-mount monopole slot antenna for handset applications as an internal penta-band WWAN antenna has been proposed. The antenna occupies a small volume of about 1.1 cm^3 only and is suitable to be surface-mounted on the main circuit board of the mobile handset. Further, the antenna is closely integrated with the system ground plane of the mobile handset, making it possible for compact integration of the antenna with nearby electronic elements. Good radiation characteristics for frequencies over the five WWAN operating bands have also been observed. The SAR results of the antenna meet the limit of 1.6 W/kg for 1-g head tissue. The proposed antenna is promising for practical mobile handset applications.

REFERENCES

1. C.I. Lin and K.L. Wong, Printed monopole slot antenna for internal multiband mobile phone antenna, *IEEE Trans Antennas Propag* 55 (2007), 3690–3697.
2. F.H. Chu and K.L. Wong, Simple folded monopole slot antenna for penta-band clamshell mobile phone application, *IEEE Trans Antennas Propag* 57 (2009), 3680–3684.
3. P. Lindberg, E. Ojefors, and A. Rydberg, Wideband slot antenna for low-profile hand-held terminal applications, *Proceedings of 36th European Microwave Conference (EuMC2006)*, Manchester, UK, pp. 1698–1701.

4. H. Wang, M. Zheng, and S.Q. Zhang, Monopole slot antenna, U.S. Patent No. 6,618,020 B2, Sep. 9, 2003.
5. S.K. Sharma, L. Shafai, and N. Jacob, Investigation of wide-band microstrip slot antenna, *IEEE Trans Antennas Propag* 52 (2004), 865–872.
6. A.P. Zhao and J. Rahola, Quarter-wavelength wideband slot antenna for 3–5 GHz mobile applications, *IEEE Antennas Wirel Propag Lett* 4 (2005), 421–424.
7. S.I. Latif, L. Shafai, and S.K. Sharma, Bandwidth enhancement and size reduction of microstrip slot antennas, *IEEE Trans Antennas Propag* 53 (2005), 994–1002.
8. W.S. Chen and K.Y. Ku, Band-rejected design of the printed open slot antenna for WLAN/WiMAX operation, *IEEE Trans Antennas Propag* 56 (2008), 1163–1169.
9. K.L. Wong and L.C. Lee, Multiband printed monopole slot antenna for WWAN operation in the laptop computer, *IEEE Trans Antennas Propag* 57 (2009), 324–330.
10. K.L. Wong and F.H. Chu, Internal planar WWAN laptop computer antenna using monopole slot elements, *Microwave Opt Technol Lett* 51 (2009), 1274–1279.
11. R. Bancroft, Dual slot radiator single feedpoint printed circuit board antenna, U.S. Patent No. 7,129,902 B2, Oct. 31, 2006.
12. C.M. Su, H.T. Chen, and K.L. Wong, Inverted-L slot antenna for WLAN operation, *Microwave Opt Technol Lett* 37 (2003), 315–316.
13. C.M. Su, H.T. Chen, F.S. Chang and K.L. Wong, Dual-band slot antenna for 2.4/5.2 GHz WLAN operation, *Microwave Opt Technol Lett* 35 (2002), 306–308.
14. K.L. Wong, Y.W. Chi, and S.Y. Tu, Internal multiband printed folded slot antenna for mobile phone application, *Microwave Opt Technol Lett* 49 (2007), 1833–1837.
15. C.H. Wu and K.L. Wong, Internal hybrid loop/monopole slot antenna for quad-band operation in the mobile phone, *Microwave Opt Technol Lett* 50 (2008), 795–801.
16. C.H. Wu and K.L. Wong, Hexa-band internal printed slot antenna for mobile phone application, *Microwave Opt Technol Lett* 50 (2008), 35–38.
17. C.I. Lin and K.L. Wong, Internal hybrid antenna for multiband operation in the mobile phone, *Microwave Opt Technol Lett* 50 (2008), 38–42.
18. American National Standards Institute (ANSI), Safety levels with respect to human exposure to radio-frequency electromagnetic field, 3 kHz to 300 GHz, ANSI/IEEE standard C95, 1999.
19. Y.W. Chi and K.L. Wong, Compact multiband folded loop chip antenna for small-size mobile phone, *IEEE Trans Antennas Propag* 56 (2008), 3797–3803.
20. C.H. Chang and K.L. Wong, Printed $\lambda/8$ -PIFA for penta-band WWAN operation in the mobile phone, *IEEE Trans Antennas Propag* 57 (2009), 1373–1381.
21. Y.W. Chi and K.L. Wong, Quarter-wavelength printed loop antenna with an internal printed matching circuit for GSM/DCS/PCS/UMTS operation in the mobile phone, *IEEE Trans Antennas Propag* 57 (2009), 2541–2547.
22. K.L. Wong and S.C. Chen, Printed single-strip monopole using a chip inductor for penta-band WWAN operation in the mobile phone, *IEEE Trans Antennas Propag* 58 (2010), 1011–1014.
23. C.T. Lee and K.L. Wong, Planar monopole with a coupling feed and an inductive shorting strip for LTE/GSM/UMTS operation in the mobile phone, *IEEE Trans Antennas Propag* 58 (2010), 2479–2483.
24. W. Yu, S. Yang, C.L. Tang, and D. Tu, Accurate simulation of the radiation performances of a mobile slide phone in a hand-head position, *IEEE Antennas Propag Mag* 52 (2010), 168–177.
25. Available at: <http://www.usb.org/>, Universal Serial Bus (USB).
26. K.L. Wong and C.H. Chang, On-board small-size printed monopole antenna integrated with USB connector for penta-band WWAN mobile phone, *Microwave Opt Technol Lett* 52 (2010), 2523–2527.
27. S.L. Chien, F.R. Hsiao, Y.C. Lin, and K.L. Wong, Planar inverted-F antenna with a hollow shorting cylinder for mobile phone with an embedded camera, *Microwave Opt Technol Lett* 41 (2004), 418–419.
28. C.M. Su, K.L. Wong, C.L. Tang, and S.H. Yeh, EMC internal patch antenna for UMTS operation in a mobile device, *IEEE Trans Antennas Propag* 53 (2005), 3836–3839.
29. K.L. Wong and C.H. Chang, Surface-mountable EMC monopole chip antenna for WLAN operation, *IEEE Trans Antennas Propag* 54 (2006), 1100–1104.
30. K.L. Wong and C.H. Chang, An EMC foam-base chip antenna for WLAN operation, *Microwave Opt Technol Lett* 47 (2005), 80–82.
31. C.M. Su, K.L. Wong, B. Chen, and S. Yang, EMC internal patch antenna integrated with a U-shaped shielding metal case for mobile device application, *Microwave Opt Technol Lett* 48 (2006), 1157–1161.
32. Available at: <http://www.ansoft.com/products/hf/hfss/>, Ansoft Corporation HFSS.
33. K.L. Wong, W.J. Chen, L.C. Chou, and M.R. Hsu, Bandwidth enhancement of the small-size internal laptop computer antenna using a parasitic open slot for the penta-band WWAN operation, *IEEE Trans Antennas Propag* 58 (2010), 3431–3435.
34. P. Vainikainen, J. Ollikainen, O. Kivekas, and I. Kelder, Resonator-based analysis of the combination of mobile handset antenna and chassis, *IEEE Trans Antennas Propag* 50 (2002), 1433–1444.
35. <http://www.semcad.com>, SPEAG SEMCAD, Schmid & Partner Engineering AG.

© 2011 Wiley Periodicals, Inc.

HETEROGENEOUS ANTHROPOMORPHIC PHANTOMS WITH REALISTIC DIELECTRIC PROPERTIES FOR MICROWAVE BREAST IMAGING EXPERIMENTS

Alireza Mashal, Fuqiang Gao, and Susan C. Hagness

Department of Electrical and Computer Engineering, University of Wisconsin, Madison, WI 53706; Corresponding author: amashal@gmail.com

Received 12 November 2010

ABSTRACT: We present a technique for fabricating realistic breast phantoms for microwave imaging experiments. Using oil-in-gelatin dispersions that mimic breast tissue dielectric properties at microwave frequencies, we constructed four heterogeneous phantoms spanning the full range of volumetric breast densities. We performed CT scans and dielectric properties measurements to characterize each phantom.

© 2011 Wiley Periodicals, Inc. *Microwave Opt Technol Lett* 53:1896–1902, 2011; View this article online at wileyonlinelibrary.com. DOI 10.1002/mop.26128

Key words: microwave imaging; breast phantoms; dielectric spectroscopy

1. INTRODUCTION

Microwave breast imaging is a nonionizing molecular imaging technique that senses the endogenous—and possibly exogenously influenced—dielectric properties of breast tissue. Microwave imaging shows much promise as a safe, low-cost, three-dimensional tomographic imaging modality. Potential applications include early-stage breast cancer detection, breast density evaluation, and cancer treatment monitoring. Definitive, quantitative validation of microwave imaging techniques is a critical component in the development of this technology. Clinical studies with human subjects provide the ultimate test domain but also pose the most challenging validation scenario due to the fact that the true in vivo properties are not known. This emphasizes the important role of realistic physical phantoms in